PERGAMON

Mechatronics 13 (2003) 933–956

MECHATRONICS

A piezoelectric driven ratchet actuator mechanism with application to automotive engine valves

Nader Jalili *, John Wagner, Mohsen Dadfarnia

Mechatronics and Automotive Research Laboratories, Department of Mechanical Engineering, Clemson University, Clemson, SC 29634-0921, USA

Received 14 December 2001; accepted 11 August 2002

Abstract

Increasing demands on the performance of internal combustion engines, specifically automobile engines, require the production of more mechanical energy for a given amount of chemical fuel with reduced tailpipe emissions. Of particular interest in the development of high performance/low emission engines is the control and timing of individual engine valves. This paper investigates the design of an innovative piezoelectric ceramic (PZT) based actuator mechanism with a novel stepping motion amplifier to deliver force and displacement at higher magnitudes and operating frequencies. The target application is an engine valve train which traditionally uses cam-based lifter driven rocker arms to regulate the cylinders' intake and exhaust valve motion. The proposed PZT-based actuator mechanism introduces a high frequency, lightweight, precise position solution for cylinder-by-cylinder variable valve timing. Numerical results are provided to demonstrate the feasibility of a PZT-based/camless valve train. The new valve train demonstrates similar cam-based performance characteristics while enabling computer controlled individual valve timing opportunities.

Keywords: Piezoelectric actuators; Mechanism design; Modeling; Valve train actuation

1. Introduction

Increasing demands on the performance of internal combustion engines, specifically automobile engines, require the production of more mechanical energy for a

* Corresponding author. Tel.: +1-864-656-5642; fax: +1-864-656-4435.
E-mail address: jalili@clemson.edu (N. Jalili).

0957-4158/03/$ - see front matter
doi:10.1016/S0957-4158(03)00009-6

Nomenclature

$\boldsymbol{A}_s$	system matrix in state-pace equation
a_m	distance between actuator attached point till pivot point in link
a_r	lever distance from left side rocker to pivot
$\boldsymbol{B}_s$	control matrix in state-pace equation
b_m	distance between ratchet attached point till pivot point in link
b_r	lever distance from right side rocker to pivot
$\boldsymbol{C}_s$	output matrix in state-pace equation
C_c	damping between second gear and rack
C_{g1}	damping between crank and first gear
C_{g2}	damping between two gears
C_{lr}	rocker damping (left side)
C_m	equivalent damping coefficient of link
C_p	push rod damping
C_{rr}	rocker damping (right side)
C_{ra}	equivalent damping between link and ratchet mechanism
d	thickness of each layer
d_{33}	electromechanical coupling coefficient
E_3	electric field in PZT
F	force acting on rocker masses due to lever
F_0	external force acting on actuator
F_a	force exerted by actuator
F_d	driving force of valve train
F_s	equivalent spring force of PZT
F_v	equivalent force of PZT from voltage
I_{g1}	moment of inertia of first gear
I_{g2}	moment of inertia of second gear
K_a	actuator stiffness
K_c	stiffness between second gear and rack
K_{g1}	stiffness between crank and first gear
K_{g2}	stiffness between two gears
K_l	stiffness between rack and lifter displacement
K_{lr}	rocker stiffness (left side)
K_m	equivalent stiffness coefficient of link
K_p	push rod stiffness
K_{ra}	equivalent stiffness between link and ratchet mechanism
K_{rr}	rocker stiffness (right side)
K_v	valve stiffness spring
l_{ra}	linkage length in ratchet mechanism
L	max height of cam profile
M	external load mass
M_{ra}	ratchet-mechanism output torque
m_a	mass of actuator

m_c	mass of rack
m_l	lifter mass
m_{lr}	rocker mass (left side)
m_{m1}	equivalent mass of link
m_p	push rod mass
m_{ra1}	equivalent mass in slider crank in ratchet mechanism
m_{ra2}	equivalent mass in slider crank in ratchet mechanism
m_v	valve stem mass
n	number of stack in actuator
N	engine rotation speed (RPM)
$\boldsymbol{r}$	displacement vector
r_l	$= r_{ra}/l_{ra}$; crank length to linkage length ratio
r_{ra}	crank length in ratchet mechanism
r_{g1}	first gear radius
r_{g2}	second gear radius
S_3	PZT strain
T_3	PZT stress
u_s	input in state-pace equation
v_a	actuator voltage
$\boldsymbol{X}_s$	state vector in state-pace equation
x_a	actuator displacement
x_c	rack displacement
x_l	lifter displacement
x_{lr}	rocker arm displacement (left side)
x_{m1}	link input displacement
x_{m2}	$= (b_m/a_m)x_{m1}$; link output displacement
x_p	push rod displacement
x_{ra}	slider displacement in ratchet mechanism
x_{rr}	rocker arm displacement (right side)
x_v	valve displacement
Y_{33}	elastic modulus of PZT
θ	crank rotation angle
θ_0	initial crank angle in ratchet mechanism
θ_1	deviation from initial crank angle in ratchet-mechanism
θ_{0c}	initial cam rotation angle
θ_{g1}	first gear angle
θ_{g2}	second gear angle
θ_{ra}	crank angle in ratchet mechanism
ϕ_{ra}	link angle in ratchet mechanism
Δt	integration time step

given amount of chemical fuel with reduced tailpipe emissions. Of particular interest in the development of high performance/low emission automotive engines is the

control and timing of individual engine valves. One attractive advantage of individual cylinder timing is the improvement in engine performance and emissions. The fresh air/fuel charge filling, and the exhaust gas expulsion out of, the cylinder may be better tailored for low and high engine speeds. For instance, the cam traditionally closes the inlet valve after bottom dead center which permits more inlet air to charge the cylinder. However, at lower engine speeds, the air momentum is insufficient to overcome the upward piston motion and a portion of the charge is rejected back into the intake manifold. In this scenario, an electronic valve closure capability would allow the valve to be shut earlier in the cycle thus retaining more charge and improving the volumetric efficiency.

Traditionally, engine valves are actuated via a cam and rocker mechanism that is directly driven by the engine (refer to Fig. 1). In this design, the valves open and close regularly during the pistons' stroke based on the cam rotation independent of other operating conditions. While the engine performance is acceptable over a wide-range of operating scenarios, the cam-driven push rods and rocker arms exhibit undesirable behaviors as the engine speed increases. Elastic deformation and impact recoil, especially valve bounce, may lead to unpredictable valve function and poor engine performance. However, opportunities exist to harness more energy by ensuring that the fuel mixture fully combusts and transmits a maximum amount of power to the drive train. By utilizing a valve system that may function independently of the cam position, the timing of each valve's opening and closing may be tuned for maximum power and efficiency in real-time.

With the widespread application of mechatronic concepts to dynamic systems in recent years, interest has been focused on the substitution of piezoelectric ceramics (PZT) for conventional electrical motors and actuators (e.g. [3]; [20] and references therein). PZTs are compounds of lead zirconate titanate and their properties can be optimized to suit specific applications by appropriate adjustment of the zirconate–

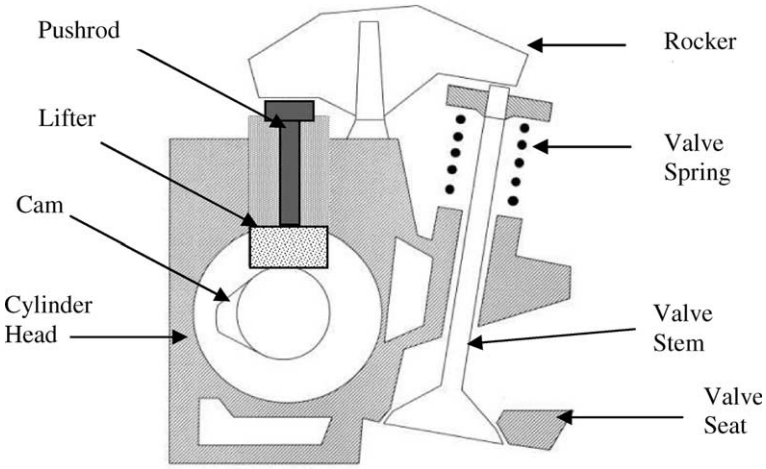

Fig. 1. Typical overhead valve assembly.

titanate ratio. Their mechanical properties make them ideal for a variety of electromechanical transducers such as generators (e.g., spark ignition, solid-state batteries), sensors (e.g., acceleration, pressure), and actuators (e.g., pneumatic and hydraulic valves). These materials initially developed for high-frequency, low displacement acoustic applications, are currently being applied to other mechanical design areas [6]. Compact and reliable, these actuators are primarily noted for their large force magnitudes. One very promising application is linear actuation.

The linear actuation market is primarily dominated by hydraulic/pneumatic cylinders and electromagnetic solenoids/shakers. However, several major drawbacks of conventional hydraulic actuators include the need for a separate hydraulic power unit equipped with an electric motor and hydraulic pump, fluid transport to the actuator from the power source, and slower response times (e.g., [4]). Pneumatic valves and cylinders offer convenient and "clean" actuation, but the available power density is much lower and the compressible air safety issue must be addressed at higher operating pressures [10]. Electrical solenoids are commonly used where full-open/full-closed position is required (e.g., poppet valves). If the pintle position must "float", then a pulse width modulated control voltage may be supplied to the coil. One of the limiting factors for solenoids is the relatively small actuation force; thus, significant opposing forces must not be presented (e.g., [18]). In hydraulic systems, the solenoid force may be magnified through the use of pilot pressures but this option may be unavailable for other applications. Finally, conventional electromagnetic shakers are generally known for their acceptable force and limited bandwidth (e.g., [15]).

A promising alternative to conventional actuation strategies are PZT devices. Many smart material applications require a large force with an accompanying large displacement. For instance, the active control of helicopter rotors and conventional flight surfaces require actuation displacements of 0.1–10 (mm) and forces of 10–10,000 (N). These requirements are often beyond the ability of single stroke actuator using either a stack or strip PZT configuration. Alternatively, the use of a well-designed displacement amplification mechanism can produce induced-strain actuators with dynamic output strokes similar to those of conventional actuators [7]. A compliant mechanism has several potential advantages including displacement magnification and reduction of backlash/Coulomb friction. However, it presents several deficiencies in comparison to conventional mechanisms such as the decreased output force due to the elasticity during retraction. Unfortunately, the bending and axial stiffness properties for conventional flexure are dependent on the same material parameters and cannot be independently designed. Thus, the problem becomes a trade-off between output force and displacement magnification. A review of existing concepts for PZT displacement magnification reveals that a multitude of methods and principles can be employed [7]. As shown in Fig. 2, a considerable amount of engineering experience has been accumulated, since the problem is not limited to PZT actuator applications.

One exciting approach for PZT actuation is the "step and repeat" motion which emphasizes the high frequency capability of the piezoelectric materials. Two actuator examples are the inch-worm linear motor [5] and the piezohydraulic pump [17]. The

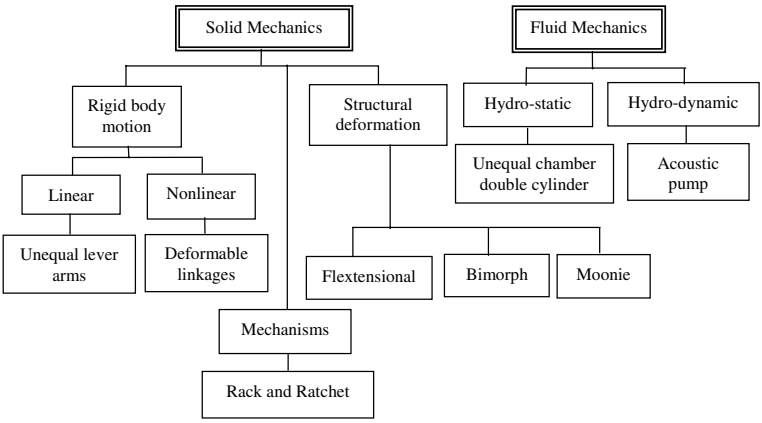

Fig. 2. Displacement amplification concepts for piezoelectric actuators.

inch-worm actuator is a cylindrical-type design consisting of three piezoceramic stack actuators and two clamping elements. They operate by incrementally summing up small micron-sized displacements into a single-large displacement. The limited induced strain of PZT material implies that one cycle will advance the device only a small amount, but the cycles may be repeated at least 100 times per cycle allowing micrometer per second velocities. The PZT pump utilizes a stack actuator to drive the piston in a miniature hydraulic pump. To compensate for the small stack displacements, system development has focused on the high frequency potential. This actuator has a 9.5 (mm) bore and achieves a 290 (N) blocking force with a free translation rate of 8.4 (mm/s). Utilizing a compliant mechanism based transmission, a piezoelectric stack actuated single-pad drum brake was recently developed [8]. A significant design component is the compliant mechanism which transmits the PZT stack actuator motion to the brake pad.

An innovative application for PZT-based actuators is the opening/closing of engine intake and exhaust valves under computer control rather than cam timing. Variable valve actuation systems offer the potential to improve torque and engine performance while lowering fuel consumption and emissions due to optimized valve timing [12]. In 1991, Demmelbauer-Ebner et al. [2] reported on various variable valve actuation systems including variable cam phasing, variable valve timing, and camshaft adjustment mechanisms with a focus on torque optimization. Morel et al. [14] investigated variable intake and exhaust cam timing on a four valve engine; results demonstrated an 11% increase in brake torque. Other studies have focused on optimizing variable valve timing for various speeds and loads (e.g., [9]). Wilson et al. [21] explored variable valve timing using an electro-hydraulic valve actuation system. In 1995, Stefanopoulou et al. [19] presented a variable cam timing controller to minimize emissions and respond to rapid throttle changes in fuel injected spark ignition engines. Their analytical work focused on fuel and cam position functionality. An enhanced model-based feedforward and adaptive feedback controller was in-

troduced by Ashhab et al. [1] to regulate the cylinder air charge of a cam free multi-cylinder engine for non-throttled operation.

Despite the recognized advantages of PZT actuation, and personal insights gained from working with piezoelectric technology, use of these actuators present significant design restrictions. The primary limitations are small deformation and nonlinear behavior. The engineering challenges lie in the development, and utilization, of these actuators for practical applications where large displacement, with accompanying high force requirements, are required. In this paper, a PZT stack actuator mechanism is proposed for high-force/large-displacement applications with high-resolution positioning. An innovative stepping motion amplifier mechanism, coupled with integrated ratchet-type transmission linkage, is designed. This PZT actuator offers an attractive alternative to conventional automotive mechanical driven actuation mechanisms in terms of greater resolution, enhanced control, and lower energy consumption.

2. Conceptual design of the proposed PZT-based valve train

Utilizing the PZT actuator's high frequency capability, a fast reciprocating displacement is first generated. The resultant displacement is then summed into a large, one-directional displacement, using a ratchet-type mechanism. This preserves the PZT actuator's large force output characteristics while magnifying its displacement. To achieve the desired output stroke, an additional lever-type motion amplifier may be integrated with a closed-loop controller for positioning accuracy. The controller will preserve the high resolution of the generated displacement by compensating for errors, nonlinearities, and environmental changes.

To offer insight into the proposed system configuration, the complete assembly is shown in Fig. 3. In this diagram, Unit 1 represents the PZT stack with intermittent motion. This motion will be amplified into one large displacement through a ratchet-type magnification mechanism to provide a usable displacement (refer to Unit 2). To provide an open/close operation similar to the conventional cam-driven valve train, a geared bi-directional mechanism is introduced in Unit 3. Finally, the generated output displacement is transferred to the stem valve in Unit 4. The functionality of each unit is described in the following subsections.

2.1. Piezoelectric actuator with stepping motion amplifier (Unit 1)

The displacement generated by a PZT actuator is relatively small with the maximum free strains for a piezoceramic on the order of 0.1%. However, the piezoceramic has a high modulus of elasticity such that the force generated by the PZT actuator will be extremely large. To generate large displacements, with a minimum loss of output force, an innovative "stepping" motion is proposed which sums smaller PZT actuator displacements. As shown in Fig. 4, the PZT either expands or contracts in proportion to the voltage (i.e. piezoelectric stress) and generates a displacement Δs_1. Applying a reverse voltage result in an actuator displacement, Δs_2, in the opposite direction. The pulse modulation of the input voltage polarity generates

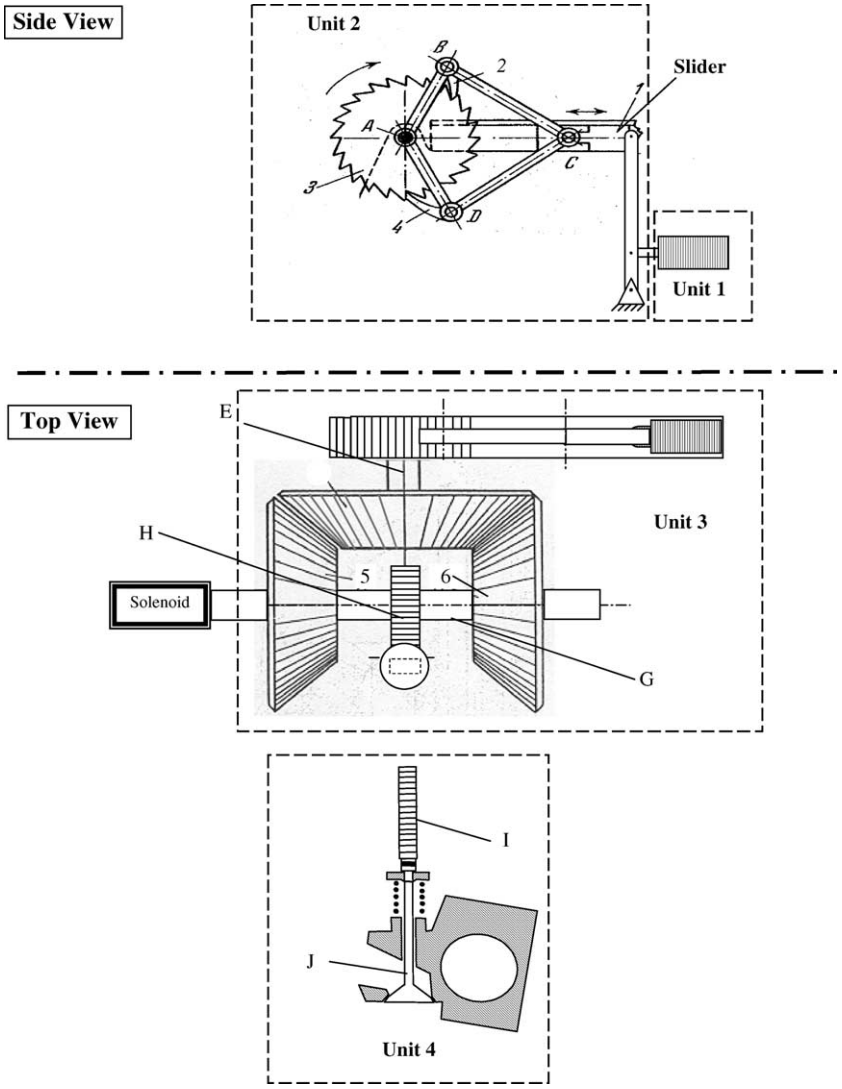

Fig. 3. Schematic of the proposed PZT-actuated engine valve.

a reciprocating motion. Due to the PZT material's fast response characteristics, the intermittent motion frequency can be kHz while the PZT tip displacement settling time can be micro seconds.

2.2. Magnification mechanism (Units 2 and 3)

Each intermittent motion step generates a reciprocating displacement. This displacement may be amplified into one large usable displacement using a ratchet-type

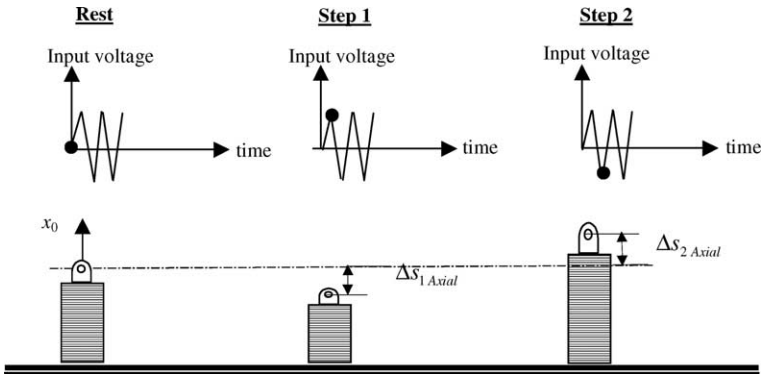

Fig. 4. Proposed PZT actuator configuration with stepping motion amplifier concept.

mechanism. While various intermittent mechanisms exist, the design presented in Fig. 3 demonstrates one possible concept. Functionally, the actuator motion will be transferred to slider 1. Slider-crank linkages ABC and ADC, with common slider 1, are connected by joints B and D to pawls 2 and 4 which engage ratchet wheel 3. When slider 1 travels to the right, pawl 2 turns the ratchet wheel 3 clockwise. Similarly, when slider 1 travels to the left, pawl 4 turns the wheel 3 in the same CW direction. Continuously changing the PZT actuator input voltage polarity ultimately results in the reciprocating motion of slider 1, and hence, rotating wheel 3 in the CW direction. In one complete stroke of slider 1 (i.e., $\Delta s_1 + \Delta s_2$), the ratchet wheel 3 rotates $\theta = 720^0/z$, where z is the number of teeth on wheel 3.

The mechanism may be attached to a geared transmission for bi-directional motion as shown in Fig. 3. In this instance, the ratchet wheel 3 is connected either directly, or with additional spur gears, to shaft E. When the one-direction rotational motion is transferred to shaft E, bevel gears 5 and 6 rotate in opposite directions about axes F and G, respectively. Gears 5 and 6 are supported on common shaft G. Their engagement is achieved through a frictional clutch acting under solenoid actuation. Pinion H is rigidly attached (i.e., keyed) to shaft G and engages rack I which is pivoted to valve J. To open the valve, the solenoid slides the shaft G to the right, and hence the connection between bevel gear 5 and shaft G is lost. Now gear 6 turns the pinion H in a CW direction. To avoid backlash, the left side of rack I may be pinned to valve J. The right side of rack I slides freely in the guide and is connected to the left side by a spring. This spring shifts the right side with respect to left side, thereby filling the tooth spaces of pinion H and eliminating backlash.

2.3. Engine valve application (Unit 4)

If attention is focused on the engine's cam driven valve train, the motion is generally specified "a priori" and cannot be readily altered. The valve timing (i.e., relative valve position versus crankshaft rotation) is dependent on the geometrical shape of the camshaft lobes on which the follower travels and effects the valves'

opening/closing. A PZT-based mechanism which operates the engine valve opening/closing events, with position feedback to monitor the stem's position, permits the individual adjustment of each cylinder's intake and exhaust valve. In this manner, the engine's volumetric efficiency may be improved at low and high speeds. The vertical displacement of rack I (refer to Unit 4 in Fig. 3) is transmitted to the valve stem J. The valve spring provides a return/resisting force to the mechanism.

3. Mathematical modeling

A suite of mathematical models will now be presented for the four units introduced in the previous section. The derivation of the governing dynamics are divided into three subsections consisting of the piezoelectric actuator, motion amplifier mechanism, and engine valve train.

3.1. Piezoelectric actuator model

Linear PZT actuators consist of a stack of many thin ceramic disks separated by metalic electrodes which alternate their connection to the voltage source positive and negative terminals (refer to Fig. 5). When activated, these electroactive disks expand, or contract, and produce extremely fine position changes (e.g. sub-nanometer range) and large forces (e.g. several 10,000 (N)) with typical strains in the range of 750–1200 (μm/m). A PZT actuator can reach its nominal displacement in approximately one-third of the resonant frequency period which permits rapid switching applications.

The one-dimensional linear electromechanical constitutive relations between the strain, S_3 the stress, T_3 and the electric field, E_3 may be expressed as [11]

$$S_3 = d_{33}E_3 + \frac{1}{Y_{33}}T_3 \tag{1}$$

where d_{33} is the linear electromechanical coupling coefficient and Y_{33} is the PZT material's elastic modulus measured at constant field. In most cases, piezo actuators

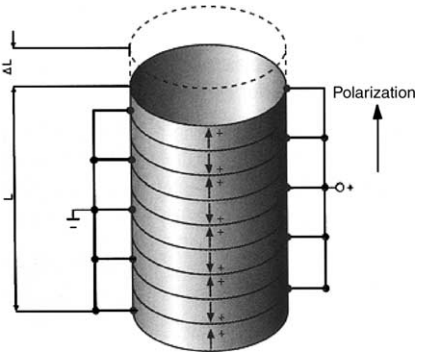

Fig. 5. Linear (stacked design) piezoelectric actuator.

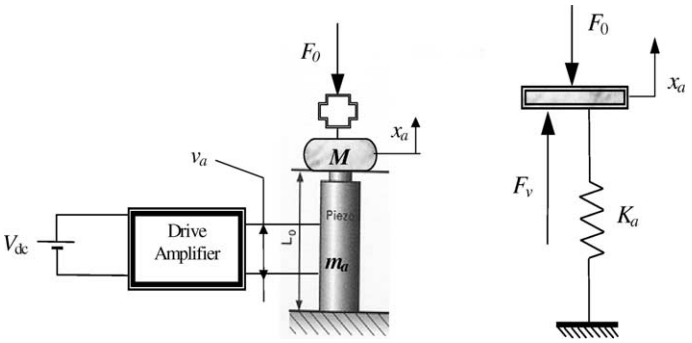

Fig. 6. PZT actuator-structure.

produce displacement. If used in a restrainted configuration, they may generate forces. Force generation is always coupled with a reduction in displacement. To simplify the analysis, linear constitutive equations are often assumed and the PZT actuator is modeled as a spring/mass system. A system level actuator description with forces, in the presence of an external mechanical load F_0, is shown in Fig. 6. The equation of motion can be written as

$$(M + m_a/3)\ddot{x}_a + F_a + F_0 = 0 \tag{2}$$

where M is the external load mass, m_a is the actuator mass, and F_a is the force exerted by the actuator. Assume that the actuator has a n-layered stack configuration (refer to Fig. 5) with each layer containing an area, A, and thickness, d. The resultant actuator stress (i.e., actuator force) may be expressed as

$$F_a = AY_{33}\left(\frac{x_a}{nd} - \frac{d_{33}}{d}v_a\right) = F_s - F_v \tag{3}$$

where

$$F_s = K_a x_a, \quad F_v = \left(\frac{AY_{33}d_{33}}{d}\right)v_a$$

and $K_a = AY_{33}/nd$ is the PZT material equivalent stiffness.

The load, or transmission mechanism, connected to the PZT has compliance that has been modeled by a linear equivalent spring and damper (refer to Fig. 7). The governing PZT equation (2) may now be stated as

$$(M + m_a/3)\ddot{x}_a = K_m(x_{m1} - x_a) + C_m(\dot{x}_{m1} - \dot{x}_a) - K_a x_a + F_v \tag{4}$$

where K_m and C_m are the equivalent spring stiffness and damping coefficient of the magnification mechanism, respectively. The variable x_{m1} represents the magnification link displacement (refer to Fig. 7). The amplifier transmission and valve stem mechanism will be considered next.

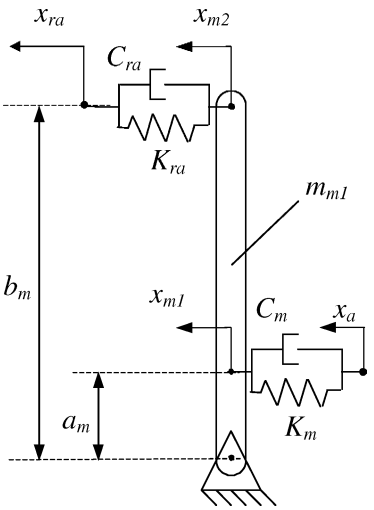

Fig. 7. Schematic of link with input and output connections.

3.2. Motion amplifier mechanism model

The Unit 2 mechanism amplifies the PZT actuator displacement using a simple link and ratchet mechanism as shown in Fig. 7. The magnification link's dynamics and kinematics are

$$m_{\mathrm{m1}}\ddot{x}_{\mathrm{m1}} = (b_{\mathrm{m}}/a_{\mathrm{m}})[K_{\mathrm{ra}}(x_{\mathrm{ra}} - x_{\mathrm{m2}}) + C_{\mathrm{ra}}(\dot{x}_{\mathrm{ra}} - \dot{x}_{\mathrm{m2}})] - [K_{\mathrm{m}}(x_{\mathrm{m1}} - x_{\mathrm{a}}) + C_{\mathrm{m}}(\dot{x}_{\mathrm{m1}} - \dot{x}_{\mathrm{a}})] \tag{5}$$

and

$$x_{\mathrm{m2}} = \left(\frac{b_{\mathrm{m}}}{a_{\mathrm{m}}}\right) x_{\mathrm{m1}} \tag{6}$$

The ratchet mechanism sums the generated reciprocative slider-crank motions, and transforms it into a rotational displacement. The two slider-crank mechanisms are symmetric, so only one needs to be modeled. The intermittent motion ratchet amplifier is divided into two parts: slider-crank mechanism, and ratchet mechanism. Let x_{ra} represent the slider-crank mechanism input, the geometric relationship between the input displacement and the output angle (refer to Fig. 8) can be expressed as

$$\theta_1 = -\theta_0 + \cos^{-1}\left(\frac{C_{\mathrm{ra}}^2 + r_1^2 - 1}{2r_1 C_{\mathrm{ra}}}\right) \tag{7}$$

where

$$C_{\mathrm{ra}} = \sqrt{1 - r_1^2 \sin^2\theta_0} + r_1\cos\theta_0 - \frac{x_{\mathrm{ra}}}{l_{\mathrm{ra}}}, \quad r_1 = \frac{r_{\mathrm{ra}}}{l_{\mathrm{ra}}} \tag{8}$$

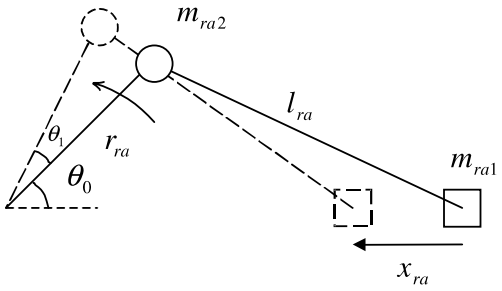

Fig. 8. Slider-crank mechanism ($\theta_{ra} = \theta_0 + \theta_1$).

In this analysis two concentrated masses, at the end of the crank and the slider point, are considered with a massless crank and arm. The equation of motion becomes

$$m_{ra1}\ddot{x}_{ra} = K_{ra}(x_{m2} - x_{ra}) + C_{ra}(\dot{x}_{m2} - \dot{x}_{ra}) - \frac{m_{ra2}r_{ra}^2\ddot{\theta}_{ra} - M_{ra}}{r_{ra}(\tan\phi_{ra}\cos\theta_{ra} + \sin\theta_{ra})} \tag{9}$$

with $\theta_{ra} = \theta_0 + \theta_1$ and

$$M_{ra} = K_{g1}(\theta_{g1} - \theta_{ra}) + C_{g1}(\dot{\theta}_{g1} - \dot{\theta}_{ra}), \quad \phi_{ra} = \sin^{-1}(r_1\sin\theta_{ra}) \tag{10}$$

Note that two slider-crank linkages are proposed for the mechanism to generate a symmetric and balanced load.

Finally, the ratchet's rotational motion is converted into a linear displacement. The equations of motion for the gears and rack (refer to Fig. 9) can be written as

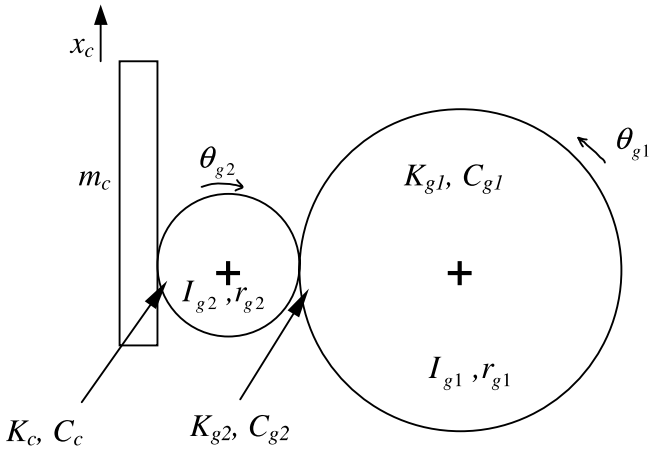

Fig. 9. Schematic of the magnification mechanism after the ratchet.

$$I_{g1}\ddot{\theta}_{g1} = K_{g1}(\theta_{ra} - \theta_{g1}) + C_{g1}(\dot{\theta}_{ra} - \dot{\theta}_{g1}) + K_{g2}\left(\theta_{g2}\frac{r_{g2}}{r_{g1}} - \theta_{g1}\right) + C_{g2}\left(\dot{\theta}_{g2}\frac{r_{g2}}{r_{g1}} - \dot{\theta}_{g1}\right) \tag{11a}$$

$$I_{g2}\ddot{\theta}_{g2} = \frac{r_{g2}}{r_{g1}}\left[K_{g2}\left(\theta_{g1} - \theta_{g2}\frac{r_{g2}}{r_{g1}}\right) + C_{g2}\left(\dot{\theta}_{g1} - \dot{\theta}_{g2}\frac{r_{g2}}{r_{g1}}\right)\right] + K_c\left(\frac{x_c}{r_{g1}} - \theta_{g2}\right) + C_c\left(\frac{\dot{x}_c}{r_{g1}} - \dot{\theta}_{g2}\right) \tag{11b}$$

$$m_c\ddot{x}_c = \frac{1}{r_{g1}}\left[K_c\left(\theta_{g2} - \frac{x_c}{r_{g1}}\right) + C_c\left(\dot{\theta}_{g2} - \frac{\dot{x}_c}{r_{g1}}\right)\right] + K_l(x_l - x_c) \tag{11c}$$

where K_{g1} and C_{g1} are the respective spring stiffness and damping coefficient between crank and ratchet (first gear). Similarly, K_{g2} and C_{g2} represent the spring stiffness and damping coefficient between the two rotating gears in Fig. 9. The parameters K_c and C_c denote the stiffness and damping coefficient between the rack and pinion.

3.3. Engine valve train modeling

The PZT-based ratchet mechanism may be applied to an automotive engine valve train. Traditionally, a cam drives the intake/exhaust valves in a fixed, periodic manner without the provision of variable timing to better accommodate operating conditions. The cam provides the cyclic displacement to drive the valve assembly based on input from a timing chain which links the crankshaft and camshaft. A lumped parameter model is presented for the engine valve train system as shown in Fig. 10 [13,16]. A variety of assumptions are imposed for the mass-spring-damper

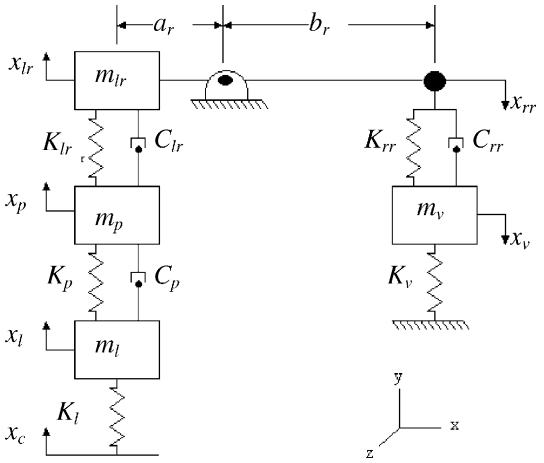

Fig. 10. Lumped parameter valve train model with ideal rocker arm.

configuration with lever transformer. First, only vertical motion is considered and the lifter and push rod are assumed to be lumped masses (i.e., m_l and m_p) with a longitudinal flexibility represented by springs and dampers. Next, the rocker arm is divided into two lumped masses (i.e., m_{lr} and m_{rr}) both possessing structural flexibility for the left and right arm sides. Non-linear friction and compliance are neglected. The valve stem is modeled as a rigid member possessing no structural flexibility or damping, and combustion induced forces on the valve face are neglected since the analysis primarily considered the "atmospheric" portion of the cycle. Finally, the rocker arm can be modeled as an ideal lever to avoid the structural analysis associated with beam deflection. Specifically, the lever connecting the left and right sides of the rocker arm is considered as a beam undergoing elastic deformation in the vertical direction. However, this modeling detail is not necessary and thus, the lever connecting the lumped rocker arm masses is considered ideal without mass or flexibility. Consequently, the right side rocker arm mass is replaced with a massless node and the majority (i.e., two-thirds) of the rocker mass.

The equation of motion for the lifter displacement, x_l, can be written as

$$m_l\ddot{x}_l = C_p(\dot{x}_p - \dot{x}_l) + K_p(x_p - x_l) + K_l(x_c - x_l) \tag{12}$$

where K_p and K_c are the push rod and cam stiffness, respectively. In this expression, C_p is the push rod damping and x_c is the cam input motion. The push rod displacement, x_p, is dependent on the push rod stiffness and rocker arm (left side) denoted by K_p and K_{lr} through

$$m_p\ddot{x}_p = C_p(\dot{x}_l - \dot{x}_p) + K_p(x_l - x_p) + C_{lr}(\dot{x}_{lr} - \dot{x}_p) + K_{lr}(x_{lr} - x_p) \tag{13}$$

where C_p and C_{lr} are the damping of the push rod and rocker arm (left side), respectively.

The vertical motion of the rocker arm (left side), x_{lr}, is considered next with the variable F denoting the lever force acting on the lumped mass, m_{lr}. The rocker arm (left side) motion is governed by

$$m_{lr}\ddot{x}_{lr} = C_{lr}(\dot{x}_p - \dot{x}_{lr}) + K_{lr}(x_p - x_{lr}) - F(b_r/a_r) \tag{14}$$

The force acting on the left and right sides of the rocker arm is function of the stiffness and damping of the rocker arm (right side) along with the motion of the valve, x_v, and the rocker arm (right side), x_{rr}, through

$$F = C_{rr}(\dot{x}_{rr} - \dot{x}_v) + K_{rr}(x_{rr} - x_v) \tag{15}$$

The motion on each side of the rocker arm, x_{lr} and x_{rr}, is linearly dependent on the other side based on the assumption of ideal lever such that $x_{rr} = (b_r/a_r)x_{lr}$ where the lengths of each side of the rocker arm from the pivoting point are denoted by a_r and b_r. The final equation of motion describes the motion of the valve, x_v, which is the variable of primary interest since it directly impacts the entering and exiting combustion gases.

$$m_v\ddot{x}_v = C_{rr}(\ddot{x}_{rr} - \ddot{x}_v) + K_{rr}(x_{rr} - x_v) - K_v x_v \tag{16}$$

4. Numerical results

The dynamic behavior of engine valves are dependent on the given powertrain and cam profile. For this numerical study, an engine operating speed of $N = 1000$ (RPM) is selected with a maximum cam displacement of 8.0 (mm) for a 180° period over the 720° crankshaft motion. A lift of 10 (mm) will be required for a PZT valve actuation mechanism. The equation that models the cam displacement, based on the input angle θ, is given by $x_c = L\pi^{-1}[\pi\theta\theta_{0c}^{-1} - 0.5\sin(2\pi\theta\theta_{0c}^{-1})]$ and displayed in Fig. 11. Eqs. (2)–(10), (11a)–(11c), (12)–(16) can be presented in the nonlinear state space form

$$\dot{\boldsymbol{X}} = \boldsymbol{A}(\boldsymbol{X})\boldsymbol{X} + \boldsymbol{B}u, \quad \boldsymbol{Y} = \boldsymbol{C}\boldsymbol{X} \tag{17}$$

where the state vectors is defined as

$$\boldsymbol{X} = \{\dot{\boldsymbol{r}}^{\mathrm{T}}, \boldsymbol{r}^{\mathrm{T}}\}^{\mathrm{T}}, \quad \boldsymbol{r} = \{x_a, x_{m1}, x_{ra}, \theta_{g1}, \theta_{g2}, x_c, x_l, x_p, x_{lr}, x_v\}^{\mathrm{T}} \tag{18}$$

and the non-zero elements of matrices $\boldsymbol{A}$, $\boldsymbol{B}$ and $\boldsymbol{C}$ are defined in Appendix A. The PZT actuator input voltage, u, is

$$u = v_a \tag{19}$$

The system dynamics is represented in MATLAB/Simulink™ [1] and the PZT actuator initiated engine valve response studied using the system parameters listed in Table 1 [13]. The integration step-size is selected as $\Delta t = 5 \times 10^{-7}$ s with a fourth-order Runge–Kutta algorithm. The small step-size reflects the small components large natural frequencies.

The PZT actuator voltage is a simple square input. The voltage's polarity changes when the ratchet wheel is rotated one step (i.e. $|x_{ra}| > 0.4$). The PZT actuator's open-loop input voltage, shown in Fig. 12, generates similar results as the cam driven valve configuration. The displacement of the actuator, link, ratchet mechanism input, and transmission gear are depicted in Figs. 13–16. In these pictures we showed how the small reciprocating motion of actuator is summed. Also, the displacement of individual valve train components are compared between the PZT-driven and cam-based valve configurations in Figs. 17 and 18. In Fig. 17 the displacement of the lifter is depicted which is half of the valve displacement drew in Fig. 18. The arm structure assumed to be rigid. For convenience, the results for the PZT-driven system are depicted for just one cycle. As expected, the response of the PZT-driven system is faster than the cam driven mechanism for each component. The residual oscillations at the end of the cycle motion in Figs. 13–18 is simply due to the open-loop nature of the controller.

PZT actuators may be operated in either an open or closed-loop manner. In an open-loop strategy, the displacement roughly corresponds to the drive voltage. This mode is ideal when the absolute position accuracy is not critical or the position is controlled by an external sensor (e.g., interferometer). Materials with a large

[1] ™Registered trademark of The MathWorks, Natick, MA.

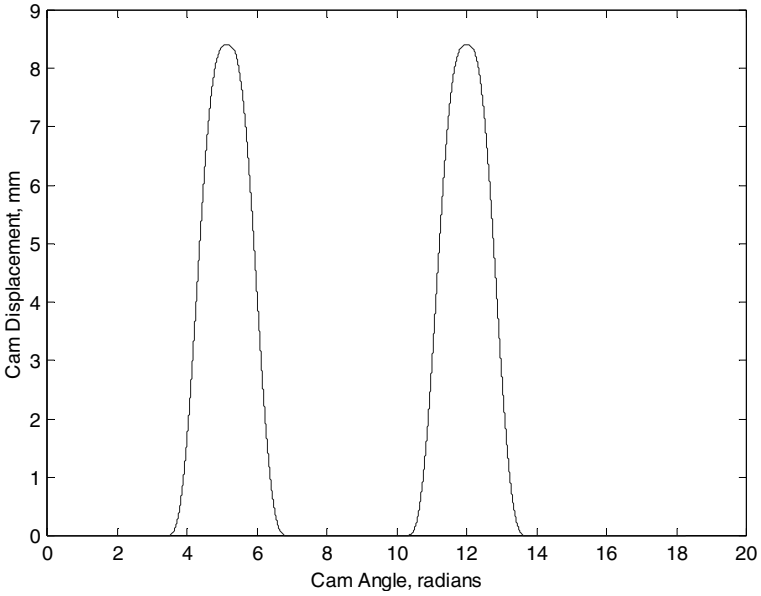

Fig. 11. Cam motion at 1000 RPM engine speed.

Table 1
System parameters used in numerical simulations

Symbol	Value	Units	Symbol	Value	Units
A	1.26×10^{-5}	(m^2)	K_l	2.0×10^7	(N/m)
a_m	0.01	(m)	K_{lr}	4.3782×10^7	(N/m)
a_r	0.0254	(m)	K_m	5×10^7	(N/m)
b_m	0.03	(m)	K_p	1.1909×10^7	(N/m)
b_r	0.0508	(m)	K_{ra}	10^7	(N/m)
C_c	66.5	(N s/m)	K_{rr}	7.5305×10^7	(N/m)
C_{g1}	66.5	(N s/m)	K_v	7.8807×10^4	(N/m)
C_{g2}	66.5	(N s/m)	M	0	(kg)
C_{lr}	66.5	(N s/m)	m_a	0.16	(kg)
C_m	66.5	(N s/m)	m_c	0.1	(kg)
C_p	66.5	(N s/m)	m_l	0.1	(kg)
C_{ra}	66.5	(N s/m)	m_{m1}	0.01	(kg)
C_{rr}	66.5	(N s/m)	m_p	0.081	(kg)
d	9.5	(mm)	m_{ra1}	0.05	(kg)
d_{33}	10^{-7}	(C/N)	m_{ra2}	0.06	(kg)
I_{g1}	1.6×10^{-4}	($kg\,m^2$)	m_v	0.091	(kg)
I_{g2}	2.0×10^{-5}	($kg\,m^2$)	n	5	–
L	8.0	(mm)	r_{g1}	0.03	(m)
l_{ra}	0.1	(m)	r_{g2}	0.02	(m)
K_a	1.6×10^7	(N/m)	r_{ra}	0.05	(m)
K_c	1.7513×10^7	(N/m)	Y_{33}	60.98×10^9	(N/m^2)
K_{g1}	5.0×10^4	(N/m)	θ_0	$\pi/6$	(rad)
K_{g2}	5.0×10^4	(N/m)	θ_{0c}	π	(rad)

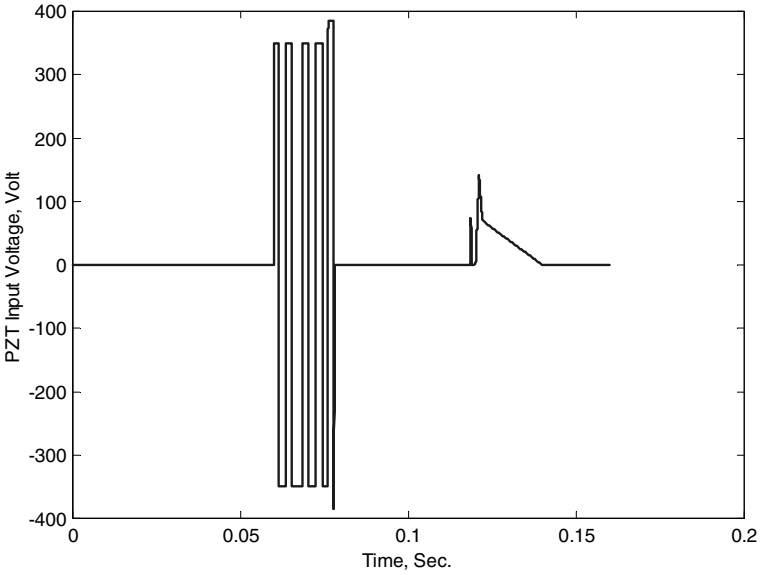

Fig. 12. Input PZT voltage in open-loop case.

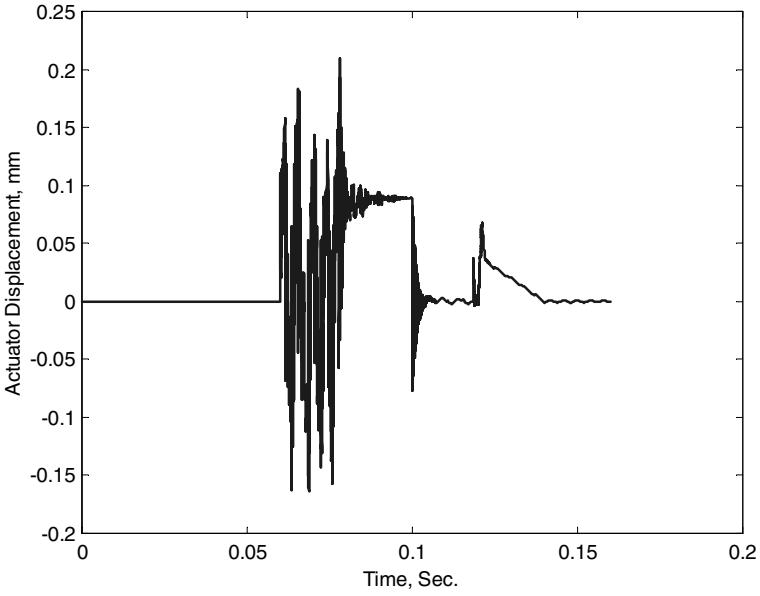

Fig. 13. Actuator displacement in open-loop case.

piezoelectric constant generally exhibit a significant hystersis for the applied voltage. For precise positioning, this hysteresis loop must be minimized. However, the

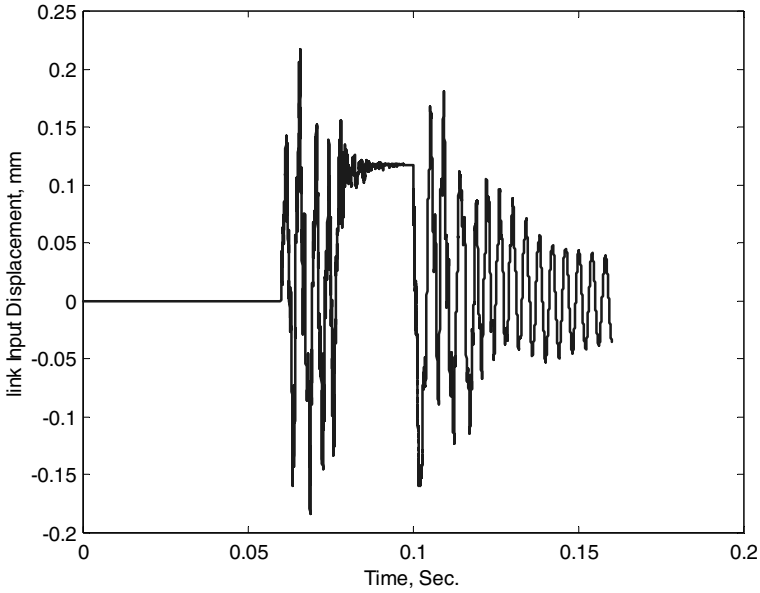

Fig. 14. Input displacement of link magnification mechanism in open-loop case.

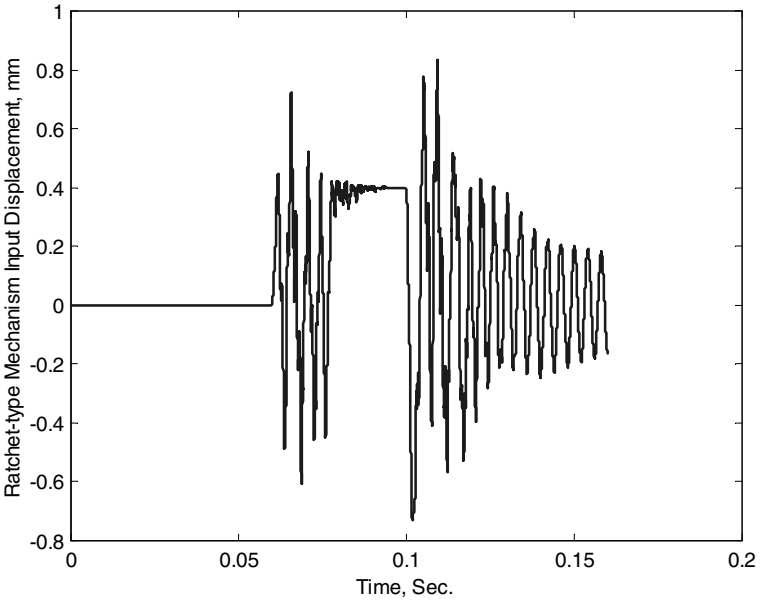

Fig. 15. Input displacement of ratchet-type mechanism in open-loop case.

development of piezoelectric materials with small hysteresis losses is difficult due to the inherent polarization effects. Accordingly, compensation should be introduced

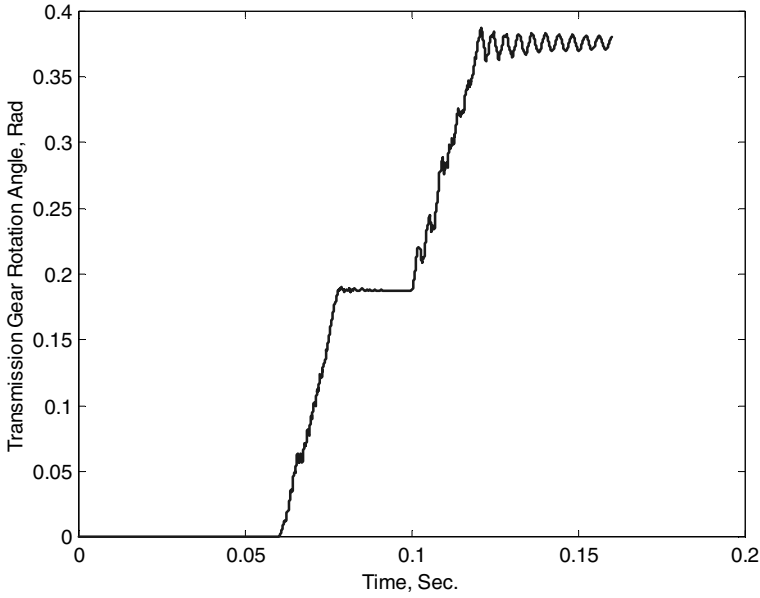

Fig. 16. Transmission gear rotation angle in open-loop case.

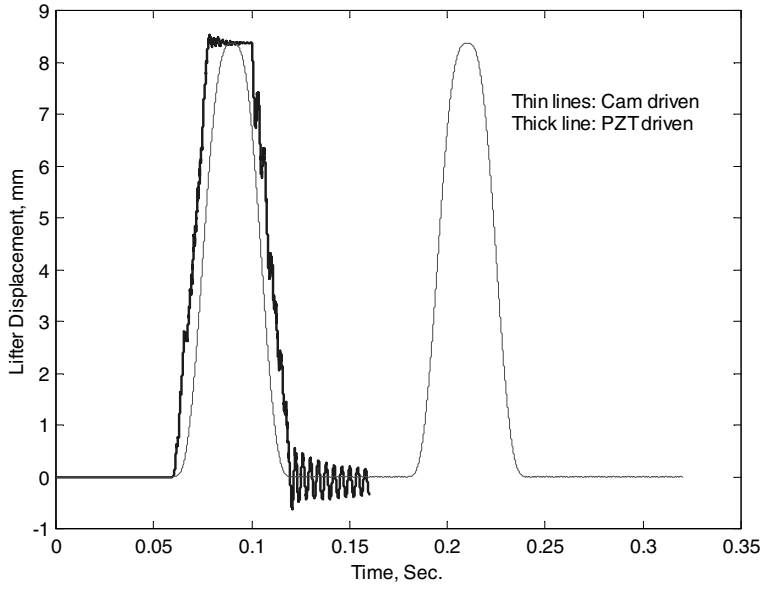

Fig. 17. Comparison of lifter displacement in cam and PZT driven system.

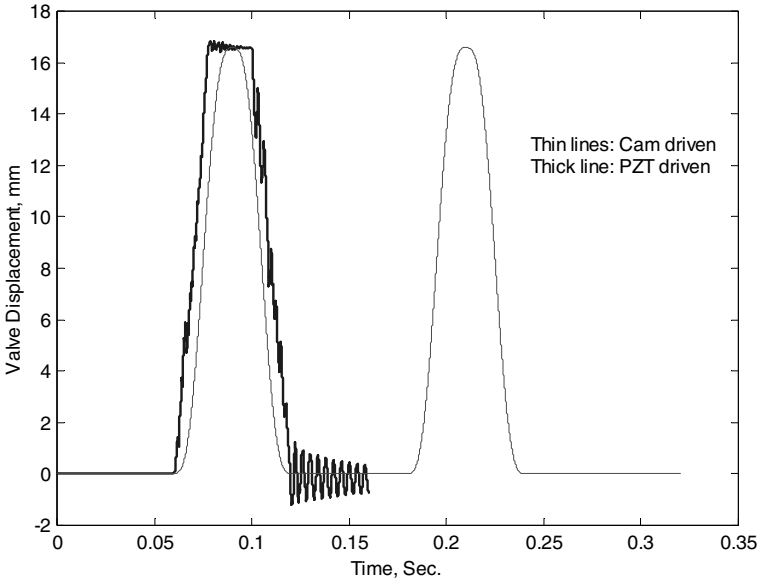

Fig. 18. Comparison of valve displacement in cam and PZT driven system.

using feedback control strategies to accommodate the material's nonlinear characteristics. Utilizing position measuring systems, a servo controller (i.e., digital or analog) will be used to determine the PZT's control signal by comparing a reference commanded position signal to the actual sensor position signal.

5. Conclusions

The design of an innovative PZT based actuator mechanism was proposed utilizing a novel stepping motion amplifier to deliver force and displacement at higher magnitudes and operating frequencies. The target application was an internal combustion engine valve train which traditionally uses cam-based lifter driven rocker arms to regulate the cylinders' intake and exhaust valve motion. The proposed PZT-based actuator mechanism offers the opportunity to introduce a high frequency, lightweight, precise positioning solution for cylinder-by-cylinder variable valve timing. Numerical results demonstrated the feasibility of the proposed PZT-based/camless valve train. The individual valve train components' responses were compared with PZT-driven and cam-based valve configurations. The response for the PZT-driven system was faster than the cam driven solution with some residual oscillations at the end of motion. Future research activities will focus on feedback control strategies to accommodate the material's nonlinear characteristics. Utilizing position measuring systems, a servo controller will determine the PZT's control signal by comparing a reference commanded position signal to the actual sensor position signal.

Appendix A

The non-zero elements of matrices $\boldsymbol{A} \in \Re^{20\times 20}$, $\boldsymbol{B} \in \Re^{20\times 1}$, and $\boldsymbol{C} \in \Re^{20\times 1}$ in Eq. (17) are

$$A_{1,1} = -\frac{C_{\mathrm{m}}}{(M + m_{\mathrm{a}}/3)} \quad A_{1,2} = \frac{C_{\mathrm{m}}}{(M + m_{\mathrm{a}}/3)}$$
$$A_{1,11} = -\frac{K_{\mathrm{m}} + K_{\mathrm{a}}}{(M + m_{\mathrm{a}}/3)} \quad A_{1,12} = \frac{K_{\mathrm{m}}}{(M + m_{\mathrm{a}}/3)}$$

$$A_{2,1} = \frac{C_{\mathrm{m}}}{m_{\mathrm{m1}}} \quad A_{2,2} = -\frac{1}{m_{\mathrm{m1}}}\left\{C_{\mathrm{ra}}\left(\frac{b_{\mathrm{m}}}{a_{\mathrm{m}}}\right)^2 + C_{\mathrm{m}}\right\} \quad A_{2,3} = \frac{C_{\mathrm{ra}}}{m_{\mathrm{m1}}}\left(\frac{b_{\mathrm{m}}}{a_{\mathrm{m}}}\right)$$
$$A_{2,12} = -\frac{1}{m_{\mathrm{m1}}}\left\{K_{\mathrm{ra}}\left(\frac{b_{\mathrm{m}}}{a_{\mathrm{m}}}\right)^2 + K_{\mathrm{m}}\right\} \quad A_{2,13} = \frac{K_{\mathrm{ra}}}{m_{\mathrm{m1}}}\frac{b_{\mathrm{m}}}{a_{\mathrm{m}}}$$

$$A_{3,2} = \frac{C_{\mathrm{ra}}}{\Delta}\left(\frac{b_{\mathrm{m}}}{a_{\mathrm{m}}}\right) \quad A_{3,3} = -\frac{1}{\Delta}\left\{C_{\mathrm{ra}} + \frac{m_{\mathrm{ra1}} r f_2(X_{13}) X_3}{S} + \frac{C_{\mathrm{g1}} f_1(X_{13})}{S}\right\}$$
$$A_{3,4} = \frac{C_{\mathrm{g1}}}{\Delta S} \quad A_{3,12} = \frac{K_{\mathrm{ra}}}{\Delta}\left(\frac{b_{\mathrm{m}}}{a_{\mathrm{m}}}\right)$$
$$A_{3,13} = -\frac{1}{\Delta}\left\{K_{\mathrm{ra}} + \frac{K_{\mathrm{g1}}}{S}\frac{f(X_{13})}{X_{13}}\right\} \quad A_{3,14} = \frac{K_{\mathrm{g1}}}{\Delta S}$$

$$S = \tan\varphi_{\mathrm{ra}}\cos\theta_{\mathrm{ra}} + \sin\theta_{\mathrm{ra}}$$
$$\theta_{\mathrm{ra}} = f(x_{\mathrm{ra}}) = \cos^{-1}\left(\frac{C_{\mathrm{ra}}^2 + r_1^2 - 1}{2 r_1 C_{\mathrm{ra}}}\right) \quad \dot{\theta}_{\mathrm{ra}} = f_1(x_{\mathrm{ra}})\dot{x}_{\mathrm{ra}} \quad \ddot{\theta}_{\mathrm{ra}} = f_1(x_{\mathrm{ra}})\ddot{x}_{\mathrm{ra}} + f_2(x_{\mathrm{ra}})\dot{x}_{\mathrm{ra}}^2$$
$$f_1(x_{\mathrm{ra}}) = \frac{\partial f(x_{\mathrm{ra}})}{\partial x_{\mathrm{ra}}} \quad f_2(x_{\mathrm{ra}}) = \frac{\partial f_1(x_{\mathrm{ra}})}{\partial x_{\mathrm{ra}}} \quad \text{and} \quad \Delta = m_{\mathrm{ra1}} + \frac{m_{\mathrm{ra2}} r f_1(X_{13})}{S}$$

$$A_{4,3} = \frac{C_{\mathrm{g1}}}{I_{\mathrm{g1}}} f_1(X_{13}) \quad A_{4,4} = -\frac{C_{\mathrm{g1}} + C_{\mathrm{g2}}}{I_{\mathrm{g1}}} \quad A_{4,5} = \frac{C_{\mathrm{g2}}}{I_{\mathrm{g1}}}\left(\frac{r_{\mathrm{g2}}}{r_{\mathrm{g1}}}\right)$$
$$A_{4,13} = \frac{K_{\mathrm{g1}}}{I_{\mathrm{g1}}}\frac{f(X_{13})}{X_{13}} \quad A_{4,14} = -\frac{K_{\mathrm{g1}} + K_{\mathrm{g2}}}{I_{\mathrm{g1}}} \quad A_{4,15} = \frac{K_{\mathrm{ra}}}{I_{\mathrm{g1}}}\left(\frac{r_{\mathrm{g2}}}{r_{\mathrm{g1}}}\right)$$

$$A_{5,14} = \frac{K_{\mathrm{g2}}}{I_{\mathrm{g2}}}\left(\frac{r_{\mathrm{g2}}}{r_{\mathrm{g1}}}\right) \quad A_{5,15} = -\frac{1}{I_{\mathrm{g2}}}\left\{K_{\mathrm{g2}}\left(\frac{r_{\mathrm{g2}}}{r_{\mathrm{g1}}}\right)^2 + K_{\mathrm{c}}\right\}$$
$$A_{5,4} = \frac{C_{\mathrm{g2}}}{I_{\mathrm{g2}}}\left(\frac{r_{\mathrm{g2}}}{r_{\mathrm{g1}}}\right) \quad A_{5,5} = -\frac{1}{I_{\mathrm{g2}}}\left\{C_{\mathrm{g2}}\left(\frac{r_{\mathrm{g2}}}{r_{\mathrm{g1}}}\right)^2 + C_{\mathrm{c}}\right\}$$
$$A_{5,16} = \frac{1}{I_{\mathrm{g2}}}\frac{K_{\mathrm{c}}}{r_{\mathrm{g1}}} \quad A_{5,6} = \frac{1}{I_{\mathrm{g2}}}\frac{C_{\mathrm{c}}}{r_{\mathrm{g1}}}$$

$$A_{6,5}=\frac{1}{m_c}\frac{C_c}{r_{g1}} \quad A_{6,6}=-\frac{1}{m_c}\left\{\frac{C_c}{r_{g1}^2}+C_l\right\} \quad A_{6,7}=\frac{C_l}{m_c} \quad A_{6,15}=\frac{1}{m_c}\frac{K_c}{r_{g1}}$$
$$A_{6,16}=-\frac{1}{m_c}\left\{\frac{K_c}{r_{g1}^2}+K_l\right\} \quad A_{6,17}=\frac{K_l}{m_c}$$

$$A_{7,6}=\frac{C_l}{m_l} \quad A_{7,7}=-\frac{C_p+C_l}{m_l} \quad A_{7,8}=\frac{C_p}{m_l} \quad A_{7,16}=\frac{K_l}{m_l}$$
$$A_{7,17}=-\frac{K_p+K_l}{m_l} \quad A_{7,18}=\frac{K_p}{m_l}$$

$$A_{8,7}=\frac{C_p}{m_p} \quad A_{8,8}=-\frac{C_p+C_{lr}}{m_p} \quad A_{8,9}=\frac{C_{lr}}{m_p} \quad A_{8,17}=\frac{K_p}{m_p}$$
$$A_{8,18}=-\frac{K_p+K_{lr}}{m_p} \quad A_{8,19}=\frac{K_{lr}}{m_p}$$

$$A_{9,8}=\frac{C_{lr}}{m_{lr}} \quad A_{9,9}=-\frac{1}{m_{lr}}\left\{C_{lr}+C_{rr}\left(\frac{b_r}{a_r}\right)^2\right\} \quad A_{9,10}=\frac{C_{rr}}{m_{lr}}\left(\frac{b_r}{a_r}\right) \quad A_{9,18}=\frac{K_{lr}}{m_{lr}}$$

$$A_{9,19}=-\frac{1}{m_{lr}}\left\{K_{lr}+K_{rr}\left(\frac{b_r}{a_r}\right)^2\right\} \quad A_{9,20}=\frac{K_{rr}}{m_{lr}}\left(\frac{b_r}{a_r}\right)$$

$$A_{10,9}=\frac{C_{rr}}{m_v}\left(\frac{b_r}{a_r}\right) \quad A_{10,10}=-\frac{C_{rr}}{m_v} \quad A_{10,19}=\frac{K_{rr}}{m_v}\left(\frac{b_r}{a_r}\right) \quad A_{10,20}=-\frac{K_v+K_{rr}}{m_v}$$

$$A_{11,1}=1 \quad A_{12,2}=1 \quad A_{13,3}=1 \quad A_{14,4}=1 \quad A_{15,5}=1 \quad A_{16,6}=1$$
$$A_{17,7}=1 \quad A_{18,8}=1 \quad A_{19,9}=1 \quad A_{20,10}=1$$

$$B_1=\frac{AY_{33}d_{33}}{d(M+m_a/3)}, \quad C_{20}=1$$

References

[1] Ashhab M, Stefanopoulou AG, Cook JA, Levin MB. Control of Camless Intake Process (Part II). Proceedings of the Dynamic Systems and Control Division, DSC 67, Nashville, TN, 1999. p. 187–94.

[2] Demmelbauer-Ebner W, Dachs A, Lenz HP. Variable valve actuation. Automot Eng 1991;99(10): 12–6.

[3] Galvagni J, Rawal B. A comparison of piezoelectric and electrostrictive actuator stacks, Paper 154–50, Adaptive and Adaptive Optical Components, SPIE 1543, 1991, p. 296–300.

[4] Gamble JB, Vaughan ND. Comparison of sliding mode control with stack feedback and PID control applied to a proportional solenoid valve. Proceedings of the ASME Dynamic systems and Controls Division, Fluids Power, Systems and Technology, vol. 1, Chicago, IL, 1994. p. 51–8.

[5] Gardner JF, Frecker M. Modeling and control of miniature inchworm actuators. Proceedings of 7th Mechatronics Forum International Conference, Atlanta, GA, 2000.

[6] Giurgiutiu V, Chaudhry Z, Rogers CA. Energy-bases comparison of solid-state induced-strain actuators. J Intel Mater Syst Struct 1996;7:4–14.
[7] Giurgiutiu V, Chaudhry Z, Rogers CA. Stiffness issues in the design of ISA displacement amplification devices: case study of a hydraulic displacement amplifier. Smart Structures and Materials, Paper # 2443-12, SPIE, vol. 2443, 1995. p. 105–19.
[8] Gogola M, Goldfarb M. Design of a PZT actuated proportional drum brake. IEEE/ASME Trans Mech 1999;4(4):409–16.
[9] Gould LA, Richeson WE, Erickson FL. Valve timing. Automot Eng 1991;99(4):19–24.
[10] Henry PJ. Safety considerations for pneumatic systems. Hydraulic Pneu 1996;49(7):47–8.
[11] Ikeda T. Fundamentals of piezoelectricity. Oxford: Oxford University Press; 1999.
[12] Jankovic M, Frischmuth F, Stefanopoulou A, Cook JA. Torque management of engines with variable cam timing. IEEE Control Syst Mag 1998;18(5):34–42.
[13] McLaughlin S. Adams Simulation of a Winston Cup Valve Train. MS Thesis, Mechanical Engineering Department, Clemson University, May 1999.
[14] Morel T, Flemming MF, Buck BA. Evaluation of variable camshaft effects on performance of a high output, 4-valve SI engine. Proceedings of the Society of Automotive Engineers, May 7–11, 1990. p. 397–433.
[15] Murray BS, Madden R, Berkman EF. Electromagnetic moving armature actuators for active vibration control. Proc ASME Noise Control Acoustics Div 1996;22(1):7–13.
[16] Norris M. Investigation of Engine Valve Dynamics and Experimental Testing of a Four-Stroke Internal Combustion Spark Ignition Engine. Research report, Mechanical Engineering Department, Clemson University, May 2001.
[17] Oates WS, Mauck LD, Lynch CS. Development of a hybrid piezoelectric hydraulic pump. Proceedings of 7th Mechatronics Forum International Conference, Atlanta, GA 2000.
[18] Rahman MF, Cheung NC, Lim KW. Position estimation in solenoid actuators. IEEE Trans Ind Appl 1996;32(3):552–9.
[19] Stefanopoulou AG, Cook JA, Freudenberg JS, Grizzle JW, Haghgooie M, Szpak PS. Modeling and control of a spark ignition engine with variable cam timing. Proceedings of the American Control Conference 4, June 21–23, Seattle, WA 1995. pp. 2576–81.
[20] Takagi T. Recent research on intelligent materials. J Intel Mater Syst Struct 1996;7:346–57.
[21] Wilson D, Watkins AJ, Dopson C. Combustion effects of asymmetric valve strategies. Automot Eng 1993;101(12):49–53.